Energy Storage Materials 63 (2023) 102980

Contents lists available at ScienceDirect

Energy Storage Materials

journal homepage: www.elsevier.com/locate/ensm

Achieving stable Zn metal anode through novel interface design with multifunctional electrolyte additive

Zhenye Liang [a,1], Chao Li [b,1], Daxian Zuo [a], Lin Zeng [a,b], Tong Ling [c], Jiajia Han [d,**], Jiayu Wan [a,b,e,*]

[a] Department of Mechanical and Energy Engineering, Southern University of Science and Technology, Shenzhen 518055, China
[b] SUSTech Energy Institute for Carbon Neutrality, Southern University of Science and Technology, Shenzhen 518055, China
[c] School of Chemistry, Chemical Engineering and Biotechnology, Nanyang Technological University, Singapore 637457, Singapore
[d] Department of Materials Science and Engineering, College of Materials, Xiamen University, Xiamen 361005, China
[e] Global Institute of Future Technology, Shanghai Jiaotong University, Shanghai 200240, China

ARTICLE INFO

Keywords:
Electrolyte additive
Nitrilotriacetic acid
Zn anode
aqueous Zn ion battery
Density functional theory

ABSTRACT

Rechargeable aqueous Zn batteries (RAZBs) are promising for energy storage systems as they are intrinsically safe, cost-effective and environmentally friendly. However, undesired dendrites and corrosion side reactions worsen at cycling, which limit the reversibility and scalable application of RAZBs. This issue arises from the undesired side reactions from corrosion of Zn in regular aqueous electrolytes, which lead to formation of side products, nonuniform Zn nucleation, finally dendrite formation. Here, we report nitrilotriacetic acid (NTA) as a highly efficient functional additive that can preferentially adsorbs on Zn surface, avoiding the direct contact between Zn and water molecules and significantly alleviating corrosion. This clean, protected Zn surface can thus promote uniform Zn plating/stripping. Furthermore, the adsorbed NTA molecules can attract water molecules to facilitate the desolvation of Zn^{2+} and promote Zn^{2+} fast transport, as verified both experimentally and computationally. Notably, we found that only a trace amount of NTA (0.15 wt%) is sufficient to form a stable electrode/electrolyte interface, reducing the corrosion rate from 3.63 mA cm^{-2} to merely 0.22 mA cm^{-2}. This stable interface enabled highly reversible Zn stripping/plating at 5 mA cm^{-2} and 0.5 mAh cm^{-2} in symmetric cells, lasting about 2100 h. An outstanding average Coulombic efficiency of 99.40 % in 800 cycles was also achieved. This study provides new insights into realizing highly reversible Zn anodes for RAZBs via the addition of highly efficient, multifunctional electrolyte additive, whose design principle may be generalized to many rechargeable battery systems.

1. Introduction

The goal of utilizing sustainable energy and electrification of transportation urges the development of energy storage devices, in which Li-ion batteries are among the most attractive choices [1–6]. Despite their high energy density, lithium-ion batteries pose a considerable safety hazard due to the utilization of flammable/explosive organic liquid electrolytes [7–10]. In contrast, rechargeable aqueous Zn batteries (RAZBs) hold great promise due to their low cost, high safety, and environmental friendliness [8,11,12]. Many technological advances aside, unfortunately, as one of the most crucial components, zinc metal anodes often suffer from poor cycling stability and low reversibility in the aqueous electrolytes. The main reasons for this problem are undesirable side reactions resulting from the direct contact of Zn surface and water, leading to the corrosion of Zn in aqueous electrolyte [13]. Subsequentially, Zn dendrite will occur during charge/discharge, resulting from uneven current distribution and Zn nucleation [14–16]. These drawbacks limit the further advancement of RAZBs, where the key to solving the aforementioned problems is to achieve uniform Zn plating/stripping. The uniform Zn deposition ensures an even distribution of electric fields, which can suppress dendrite formation by promoting uniform Zn nucleation and growth. In addition, a flat surface reduces the

* Corresponding author at: Global Institute of Future Technology, Shanghai Jiaotong University, Shanghai 200240, China.
** Corresponding author.
E-mail addresses: jiajiahan@xmu.edu.cn (J. Han), wanjy@sjtu.edu.cn (J. Wan).
[1] These authors contributed equally to this work.

https://doi.org/10.1016/j.ensm.2023.102980
Received 23 June 2023; Received in revised form 5 September 2023; Accepted 16 September 2023
Available online 17 September 2023

surface area to minimize side reactions [17,18].

Researchers have adopted various methods in achieving this goal, such as artificial electrode/electrolyte interphase design, electrolyte engineering, external field regulation, the architecture design of Zn anode or current collectors, etc [19]. Among these, electrolyte engineering is a simple and effective method of stabilizing zinc anodes in aqueous electrolytes where the utilization of electrolyte additives is considered one of the most cost-effective and efficient ways to tackle the abovementioned problems [20]. Typical electrolyte additives can be mainly classified into two categories, including inorganic and organic additives. Inorganic salt (e.g., $PbSO_4$ [21], $NiSO_4$ [22,23], $CuSO_4$ [24], Na_2SO_4 [25,26], LiCl [27,28]) is a typical class of inorganic additives that can effectively inhibit Zn dendrites through ion adsorption and electrostatic shielding [26,29]. Moreover, inorganic salt can also serve as a bifunctional additive, such as $MnSO_4$, which not only inhibits Zn dendrites but also inhibit the dissolution of Mn^{2+} ions from the manganese dioxide cathode, widely studied by various research groups [30–32]. However, inorganic salt additives usually cannot hamper side reactions, such as hydrogen evolution and Zn corrosion, which only partially solve the problem. Organic additives possess one of the richest diversity, including small molecules, polymers, ions, organic acids, and surfactants. Many organic additives have a surface tension effect, especially surfactants, which can be readily adsorbed at the interface between the electrode and the electrolyte [33]. This interfacial layer naturally blocks the direct contact of the Zn metal surface with water molecules, thus serving as a protection layer for Zn anode. However, while the use of organic additives improves the stability of the zinc anode, the additional layer may increase the difficulty in Zn-ion desolvation, leading to the increase of polarization compared with non-additive electrolytes, which may result in battery failure at large current density. Despite various successful reports, a multifunctional additive that not only alleviates Zn corrosion and suppress dendrite, but also reduces polarization is yet to be developed to complement previous studies.

Here, we introduce the utilization of nitrilotriacetic acid (NTA) as an effective electrolyte additive addressing the above concerns and study its effects and mechanisms experimentally and computationally. NTA is conventionally known for metal pollution treatment and anti-corrosion industries for its ability to form strong coordination bonds with metal (ions) and biodegradable characteristics [34–36]. In this work, we demonstrated that only a trace amount of NTA (0.15 wt%) as an electrolyte additive could effectively form an anode/electrolyte interphase, leading to excellent electrochemical performance. In the NTA-added aqueous electrolyte, the corrosion reaction rate of the Zn anode is decreased by 93.9 %, meanwhile, the polarization voltage of Zn deposition is surprisingly reduced significantly. The symmetric cell exhibits a stable electrochemical performance of 2100 h in plating/stripping cycles at high current density (5 mA cm^{-2}), much longer than the Zn||Zn symmetric cell (46 h) with regular $ZnSO_4$ electrolyte. Our study provides a facile and efficient method for improving the reversibility and stability of Zn metal anode via the introduction of stable interfacial chemistry between NTA and Zn anode. We hope the understanding of the mechanism can serve as one of the guiding principles for future electrolyte innovation in rechargeable batteries.

2. Results

The typical reactions at the Zn anode/electrolyte interface without/with NTA additive can be illustrated in Fig. 1a and 1b, respectively. In normal aqueous electrolytes (Fig. 1a), due to the direct contact between

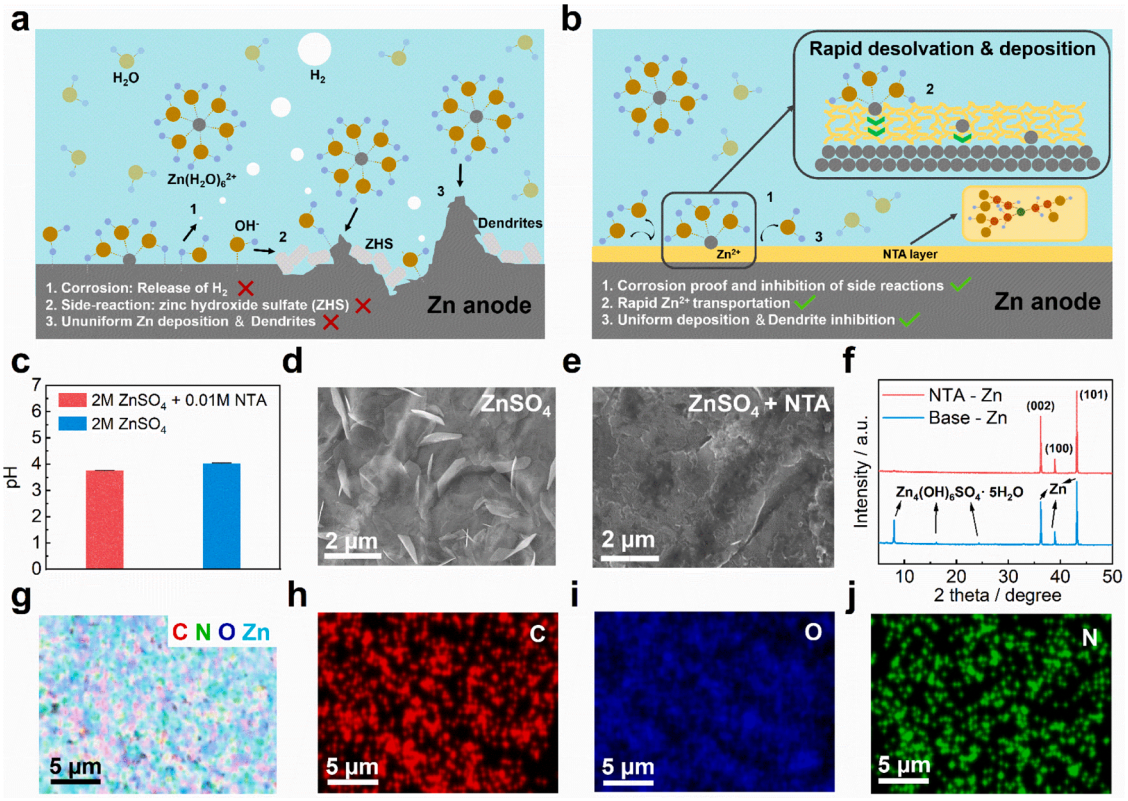

Fig. 1. Schematic diagram and experimental results of NTA on the Zn anode. Schematic illustration of electrochemical zinc plating on Zn electrodes in (a) typical $ZnSO_4$ electrolyte (NTA-free) and (b) $ZnSO_4$ electrolyte with NTA additive. (c) pH chart of 2M $ZnSO_4$ electrolyte and 2M $ZnSO_4$ + 0.01M NTA electrolyte. SEM images of a Zn foil surface after immersion in (d) 2M $ZnSO_4$ electrolyte and (e) 2M $ZnSO_4$ + 0.01M NTA electrolyte for three days. (f) XRD results of Zn foil after immersion in the NTA-free and NTA-added aqueous electrolytes for three days. EDS mapping of Zn surface after NTA-added electrolyte immersion: (g) overall, (h) C, (i) N, and (j) O elements distribution results.

water molecules and Zn metal, the active Zn metal usually undergoes a corrosion reaction with water which leads to hydrogen evolution reaction (HER). Meanwhile, due to the loss of H^+ in HER, the local pH value of the Zn metal anode surface is significantly increased, leading to the generation of non-conductive zinc hydroxide sulfate (ZHS) sheets. This undesirable ZHS will largely increase polarization at the Zn electrode surface, resulting in nonuniform current density and uneven Zn striping/plating on the electrode surface, and finally, zinc dendrites formation after cycling [37,38]. To solve the above problems, an NTA electrolyte additive is introduced, and its effect is illustrated in Fig. 1b. Instead of water molecules, NTA will be preferentially adsorbed on the surface of the Zn anode to form a protective layer, which can reduce the direct contact between active zinc and water molecules, thereby inhibiting the side reactions, including corrosion. In addition, the existence of NTA will assist the desolvation process of Zn^{2+}, which will lower the nucleation barrier and facilitate the transport and uniform deposition of Zn^{2+} at the Zn surface. Due to the above two effects of simultaneously corrosion-proof and fast desolvation, NTA could serve as a highly desirable electrolyte additive. The stability and reversibility of Zn anode in NTA-containing electrolyte are expected to be significantly improved. It should be noted that the addition of NTA to the electrolyte may cause a decrease in pH, which could potentially harm the Zn anode. To investigate this, we measured the pH of the 2M $ZnSO_4$ electrolyte and the 2M $ZnSO_4$ + 0.01M NTA electrolyte, as shown in Figs. 1c and S1, respectively. The results show a slight decrease in pH after the addition of NTA (from 4.03 to 3.75), which can be attributed to the carboxyl group of NTA. However, the decrease in pH is negligible due to the small amount of NTA used. The small amount of NTA used results in a negligible decrease in pH. This decrease in pH is generally considered harmful to the Zn metal. However, NTA can form a stable protective layer on the surface of the Zn anode, preventing direct contact between the electrolyte and the electrode. This protective layer stabilizes the Zn anode. Therefore, the slight decrease in pH caused by NTA does not harm the Zn metal. Instead, it is the structural properties of NTA that provide the protective effect, which will be further discussed below.

To study the effect of NTA molecules on Zn metal, we first immersed Zn into the two electrolytes and kept it for three days, after which their SEM images were taken and shown in Fig. 1d and 1e, respectively. Compared with the fresh Zn metal anode, which was flat and smooth (Fig. S2), the surface of the soaked Zn metal anode (in the NTA-free electrolyte, 2M $ZnSO_4$) became rough. We observed six edge-shaped sheet-like products due to the formation of ZHS by the corrosion side reactions (Fig. 1d). In contrast, the surface of the Zn metal electrode was nearly unchanged after being immersed in 2M $ZnSO_4$ + 0.01M NTA (NTA-added) electrolyte for three days. The surface was flat and had no observable side products (Fig. 1e), which may be protected by the adsorption layer formed by NTA on the surface of Zn anode. We also verified the composition of the side products with X-ray diffraction (XRD), in which the NTA group was absent of ZHS while the control group shows a strong ZHS signal (Fig. 1f). In addition, we carried out Energy Dispersive Spectroscopy (EDS) mapping to the dry Zn metal soaked in NTA-additive electrolyte (Fig. 1g–1j). We observed the existence of C, N, and O elements (main elements in NTA), which were uniformly distributed on Zn, proving the existence of the NTA

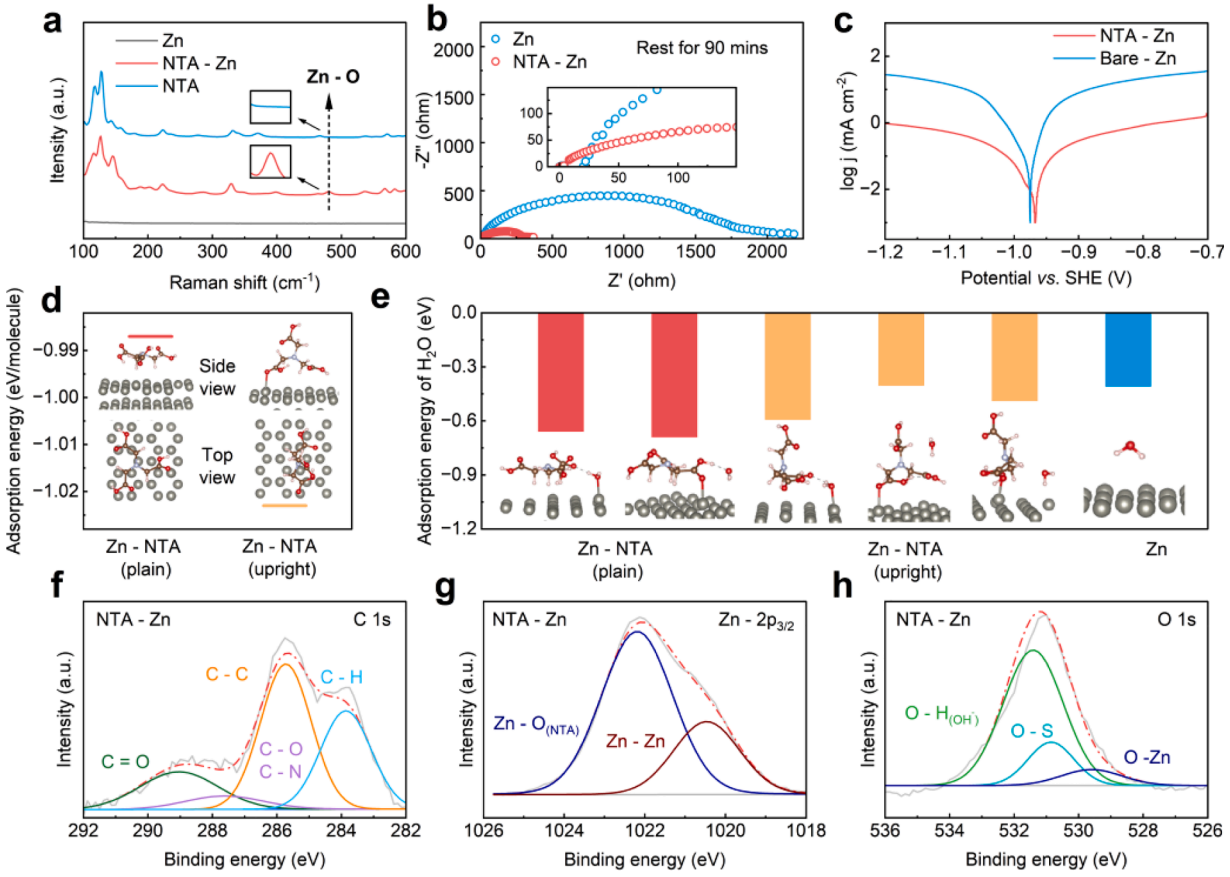

Fig. 2. Characterization of NTA adsorption on Zn and its mechanistic studies. (a) Raman spectra of pristine Zn electrode, NTA powder, and Zn electrode after rapid treatment in NTA-added electrolyte. (b) Electrochemical impedance spectroscopy (EIS) results of Zn||Zn symmetric cells in 2M $ZnSO_4$ or 2M $ZnSO_4$ + 0.01M NTA electrolyte after 90 min. (c) Linear polarization curves of Zn||Zn symmetric cells in 2M $ZnSO_4$ and 2M $ZnSO_4$ +0.01M NTA electrolytes. (d) Adsorption energy of NTA on Zn surface with two configurations, namely L-Zn-NTA and S-Zn-NTA. (e) Adsorption energy of H_2O on the L-Zn-NTA, S-Zn-NTA and Zn, respectively. (f) High-resolution XPS spectra of C 1s with Zn plated from NTA-added electrolyte. High-resolution XPS spectra of (g) Zn $2p_{3/2}$ and (h) O 1s after Zn electroplating from NTA-added electrolytes.

adsorption layer on the surface of the Zn anode. Therefore, we demonstrated that the NTA electrolyte additive could effectively inhibit corrosion on the Zn metal surface.

We studied the mechanism and its protective effect of chemisorbed NTA molecules on the Zn metal surface. We prepared a dry NTA-Zn sample by immersing a piece of Zn metal in NTA solution, quickly taking it out, washing with deionized water and drying it. By analyzing the Raman spectrums of pure NTA and NTA-Zn surfaces in Fig. 2a, we observed that NTA-Zn has a new peak at 480.6 cm^{-1}, which can be identified as the Zn-O vibration peak [33,39]. This observation indicates that NTA can be firmly adsorbed on the surface of Zn. Next, we examined the electrochemical impedance spectroscopy (EIS) of Zn symmetrical cells with NTA-free and NTA-added aqueous electrolytes after 90 min of resting, respectively [40]. As shown in Fig. 2b, the Zn||Zn symmetric cell with NTA-added electrolyte obtained a much smaller bulk and charge transfer resistance than NTA-free electrolyte due to the suppressed ZHS product. Furthermore, linear polarization measurement was taken to quantitatively analyze the corrosion rate of Zn metal in different electrolyte environments. As shown in Fig. 2c, the corrosion current density of the Zn anode in the NTA-added electrolyte (0.22 mA cm^{-2}) was much lower than that in the NTA-free electrolyte (3.63 mA cm^{-2}), indicating much-suppressed corrosion with the NTA additive (details see Methods) [33,41].

We then carried out density functional theory (DFT) calculations to verify and understand the atomic configuration of NTA on the Zn surface. Through structural optimization, we found that NTA has two thermodynamically stable states, namely L-Zn-NTA (lying flat) and S-Zn-NTA (standing up), as shown in the inset of Fig. 2d. The calculated adsorption energy of L-Zn-NTA is -0.987 eV, and that of S-Zn-NTA is -1.023 eV, respectively, which are close to each other. Such close adsorption energy indicates that both appear with comparable probability. The results of charge density difference and bader charge analysis result (Fig. S3) show that there is no significant charge transfer between NTA and the Zn surface, which remains the typical metal characteristics contributed from Zn-4s and Zn-4p orbits (Fig. S4 DOS). We further investigated the interaction of Zn with NTA (H_2O) and calculated their adsorption energy on the Zn surface (Fig. 2e). We note that the adsorption energy of NTA is lower than that of H_2O, indicating that NTA can be adsorbed to the Zn surface preferentially over H_2O, thus alleviating the corrosion side reactions. In addition, that the NTA attached to the Zn surface has lower adsorption energy for H_2O than the Zn surface at all spatial directions, which further indicates the increased difficulty of corrosion side reaction on the Zn surface adsorbed by NTA.

The presence of NTA on the Zn anode after electrochemical plating was further characterized by X-ray Photoelectron Spectroscopy (XPS), in which the characterized Zn anodes were electroplated under the conditions of 10 mA cm^{-2} in either NTA-added or NTA-free electrolytes, respectively. In the full survey spectrum (Fig. S5), the presence of C, O, Zn, and S on the electrode can be identified. For the high-resolution spectra of C 1s, the bare-Zn treated in NTA-free electrolyte only exhibits typical bonds of C-O and C=O (Fig. S6). In contrast, the Zn anode treated with NTA-added electrolyte (NTA-Zn) exhibits a strikingly different behavior with C–H, C–C, C–O/C-N, and C=O at 283.9, 286.8, 287.6, and 289.1 eV, respectively (Fig. 2f). In contrast, the electrolyte-treated zinc foil without NTA did not exhibit the characteristic C-H peak (Fig. S6). Although the presence of N element in the full spectrum is unclear, the typical bond of N-C (399.3 eV) is evident from the high-resolution spectrum of N 1s (Fig. S7) [42]. The analysis above suggests that NTA exists and remains on the surface of Zn anode during the plating/stripping process. The high-resolution spectra of Zn 2p showed that for both groups, with and without NTA in the electrolyte, exhibited Zn-Zn and Zn-O peaks (Figs. 2g and S8). However, the Zn-O peak on the surface of Zn anode of the NTA-added group was significantly higher than that of the group without NTA, and there were also differences in the peak positions of the two groups. This difference occurred because the Zn-O peak on the surface of the NTA-added group resulted from the chemisorption of NTA with Zn, whereas the Zn-O peak of the group without NTA resulted from the side reaction product ZHS [43]. Additionally, the O 1s spectra of NTA-Zn revealed the existence of O-Zn in addition to O-H (OH^- in ZHS) and O-S (from SO_4^{2-} in ZHS), which demonstrated the chemical adsorption of NTA on the surface of Zn (Fig. 2h). However, O-Zn was not observed in the O 1s spectra of the Zn anode plated in NTA-free electrolyte as a control group (Fig. S9). It is worth noting that although NTA has a strong protective effect on the Zn anode, it may not completely inhibit the side reactions. Therefore, the presence of ZHS was also observed in the O 1s spectra of the NTA-added Zn group [42]. These results indicate the existence of NTA on the Zn surface and demonstrate that NTA is not reduced during the Zn plating process. The chemical adsorption of NTA on the surface of the Zn anode was once again proven.

To verify the protective effect of NTA on the Zn anode, we performed Coulomnic efficiency (CE) tests with Zn||Cu cells [44]. Fig. 3a shows the average CE values for the Zn||Cu cell with and without NTA. It is cleared that the CE of the Zn||Cu cell with NTA is significantly higher than the one without NTA. Additionally, it is observed that the nucleation overpotential of Zn is reduced after adding NTA. Fig. 3b summarizes the CE and nucleation overpotential results and demonstrates that the addition of NTA leads to a significant improvement in CE and a decrease in nucleation overpotential. The increase in CE is attributed to the formation of a protective layer by NTA on the electrode surface, which inhibits contact between Zn and H_2O, thus preventing Zn from participating in side reactions [45]. The reduction in the nucleation overpotential may come from the blocking-free (without ZHS) and water-grabbing characteristics of the NTA-modified Zn surface, where the desolvation process of Zn^{2+} is much easier [46]. We further characterized the Zn surface after electrochemical plating to verify whether the NTA additive can suppress the dendrite formation. From Fig. 3c, we can directly observe the black product (this product may be caused by uneven deposition of Zn) generated on the Zn surface (under 10 mAh cm^{-2} current density) in the NTA-free electrolyte. In contrast, the morphology of the Zn surface after Zn plating in the NTA-added electrolyte maintained uniform and dense, without observable by-products. From the crystallographic point of view, Zn should orient at the (002) plane for a favorable uniform Zn deposition compared with the (100) orientation [47]. As shown in Fig. 3d and Table S1, the ratio of (100) and (002) diffraction peak intensities of the Zn electrode from NTA-added electrolyte after plating is 0.24, which is lower than the electroplated Zn electrode (0.34) in NTA-free electrolyte and fresh Zn electrode (0.28). These results indicate that after NTA addition, Zn is less likely to form dendrites [47,48]. We further investigated the Zn plating process in different electrolytes using SEM. As shown in Fig. 3e, the surface of the Zn electrode in NTA-free electrolyte became rough and uneven, with obvious dendrites formed from the irregular deposition of Zn^{2+}. In contrast, the Zn electrode in NTA-added electrolyte was dense, flat, and uniform, presenting the strong tunability of NTA additive for uniform Zn deposition (Fig. 3f).

Due to the excellent corrosion/dendrite inhibition and polarization reduction effect of NTA additive to Zn plating, we anticipated a stable Zn plating/stripping behavior in symmetrical cells. Therefore, we performed battery cycling and investigated NTA's effect on the Zn anode's stability and reversibility. As shown in Fig. 4a, at 5 mA cm^{-2} and 0.5 mAh cm^{-2}, the Zn||Zn symmetric cell with NTA-added electrolyte had a low polarization of about 46 mV and cycle life as long as 2100 h (Fig. S10). In contrast, the NTA-free electrolyte control group only cycled less than 100 h and polarized as high as 200 mV before failure. At high cycling current density (10 mA cm^{-2}) and capacity (2 mAh cm^{-2}), the Zn||Zn symmetric cell with NTA-added electrolyte still had a low polarization of about 50 mV and a long cycle life of 500 h (Figs. 4b and S11). In contrast, the Zn||Zn symmetric cell with NTA-free electrolyte kept increasing polarization until it failed at merely 80 h. We further demonstrated the rate performance of the two electrolytes of the symmetrical cells, as shown in Fig. 4c. We observed that compared with the

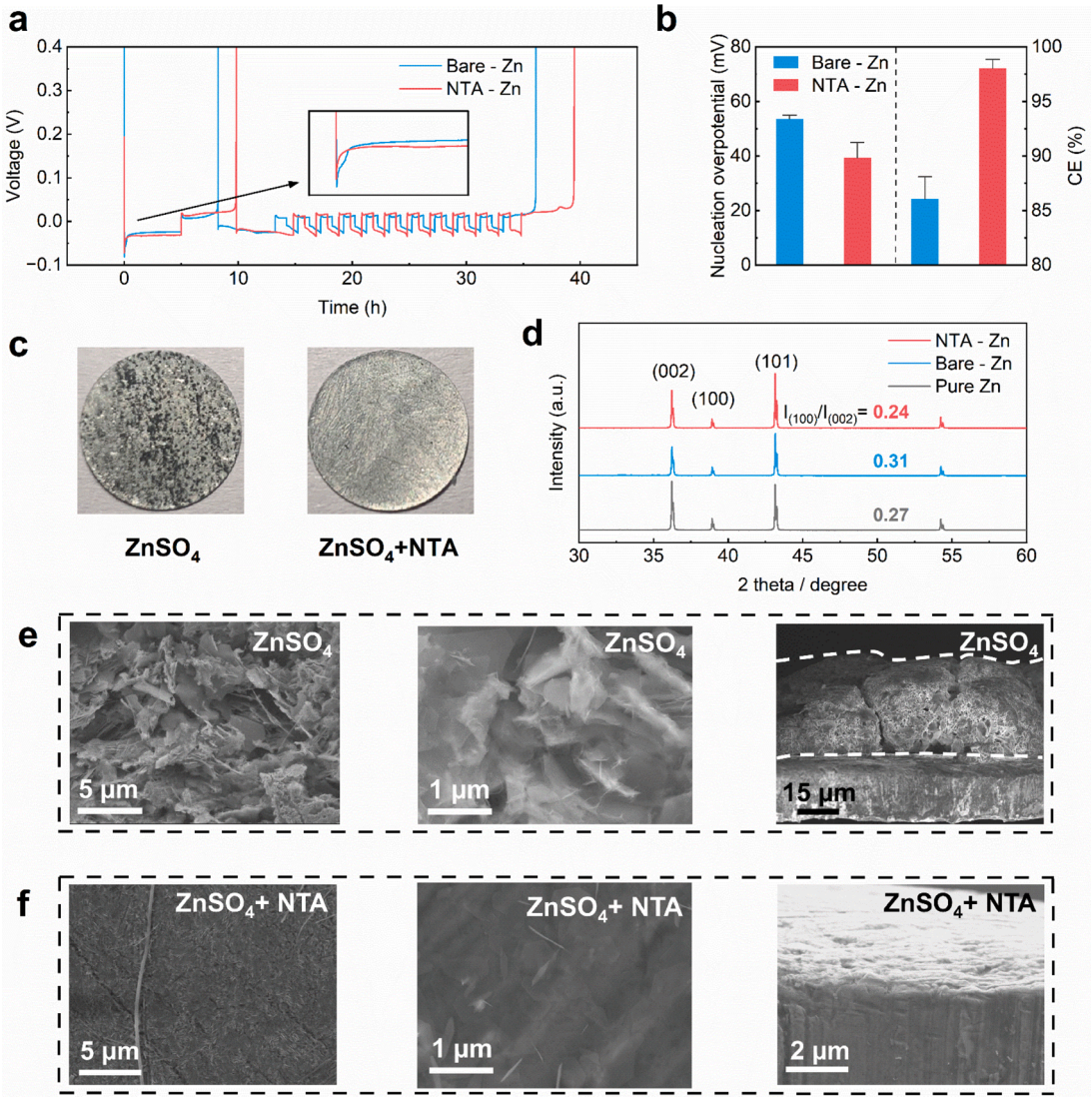

Fig. 3. Characterization and test of Zn surfaces after Zn metal plating with the two different electrolytes. (a). Representative voltage profiles from Zn||Cu cells with/without NTA for measuring CE at 1 mA cm^{-2}. The inset is a magnified image of voltage profiles to show the overpotential difference with the tested electrolytes. (b) Averaged CE and nucleation overpotential values from $ZnSO_4$, $ZnSO_4$ + NTA. (c) Photos of Zn electrodes after electroplating 10 mAh cm^{-2} Zn metal in 2M $ZnSO_4$ electrolyte and 2M $ZnSO_4$ +0.01M NTA electrolyte. (d) XRD analysis of fresh Zn metal and Zn anode after plating in 2M $ZnSO_4$ electrolyte and 2M $ZnSO_4$ + 0.01M NTA electrolyte. SEM images of Zn electrodes after electroplating 10 mAh cm^{-2} Zn metal in 2M $ZnSO_4$ electrolyte (e) and 2M $ZnSO_4$ +0.01M NTA electrolyte (f).

2M $ZnSO_4$ electrolyte, the Zn||Zn symmetric cell with 2M $ZnSO_4$ + 0.01M NTA was stable up to 20 mA cm^{-2} current densities with lower polarization. To explore the effect of NTA on the reversibility toward anodeless Zn metal batteries, Zn||Cu cells were used to measure the Coulombic efficiency (CE). As shown in Fig. 4e, the CE of Zn||Cu cells with NTA additive was as high as 99.40 % and cycled for 810 cycles at 1 mA cm^{-2} and 1 mAh cm^{-2}. However, the CE of the control Zn||Cu cell without NTA dropped significantly after merely 70 cycles, indicating massive side reactions and dendrite formation. At 2 mA cm^{-2} and 2 mAh cm^{-2}, the CE of Zn||Cu cells with NTA additive was as high as 99.60 % and cycled for 520 cycles, but the CE of the control Zn||Cu cell without NTA dropped significantly after merely 46 cycles (Fig. 4e). In addition, the self-discharge behavior of the Zn||Cu cell was also tested, in which we plated Zn at the Cu surface, held for 0/24/48/72 h, and stripped the remaining Zn (Fig. 4f). We observed that after standing for four periods, the CEs of Zn||Cu cells with NTA additive electrolyte were higher than those of Zn||Cu cells with NTA-free electrolyte, again indicating the NTA additive can alleviate the corrosion of plated Zn. Finally, we compared representative studies of ZIB (with electrolyte engineering) and specifically count the polarization and cycle life of different additives/electrolytes at 5 mA cm^{-2} [17,33,41,45,46,48–52]. Our work has a relatively long cycle life and low polarization (Fig. 4g), which is at the frontier of state-of-the-art results.

The excellent cycling behavior of Zn symmetrical cells with NTA-added electrolyte could be understood macroscopically with the relatively fresh and clean Zn surface, and the NTA-assisted fast Zn^{2+} transport channel. In comparison, the Zn anode surface is covered (blocked) with ZHS in the NTA-free electrolyte. However, the atomistic mechanism of NTA at the Zn surface is still missing. We further carried out DFT calculations to study the kinetic behavior of foreign Zn^{2+} on the Zn surface with or without NTA adsorption. The nudged elastic band (NEB) results show that with the existence of NTA, the as-deposited Zn obtained a higher diffusion barrier than that on the bare Zn surface as shown in Fig. 5a (red and orange curve, labeled “near”.). This suggests that NTA has an inhibitory effect on the diffusion of Zn^{2+} and prevents the aggregation of originally dispersed Zn^{2+}. The Zn far from the NTA molecule (red and orange dotted line labeled “far”) shows a much flatter diffusion barrier, indicating the effective zone of diffusion inhibition was calculated within three Zn atomic layers (from NTA). Fig. 5b–5d further illustrate the trend of potential dendrite formation during Zn

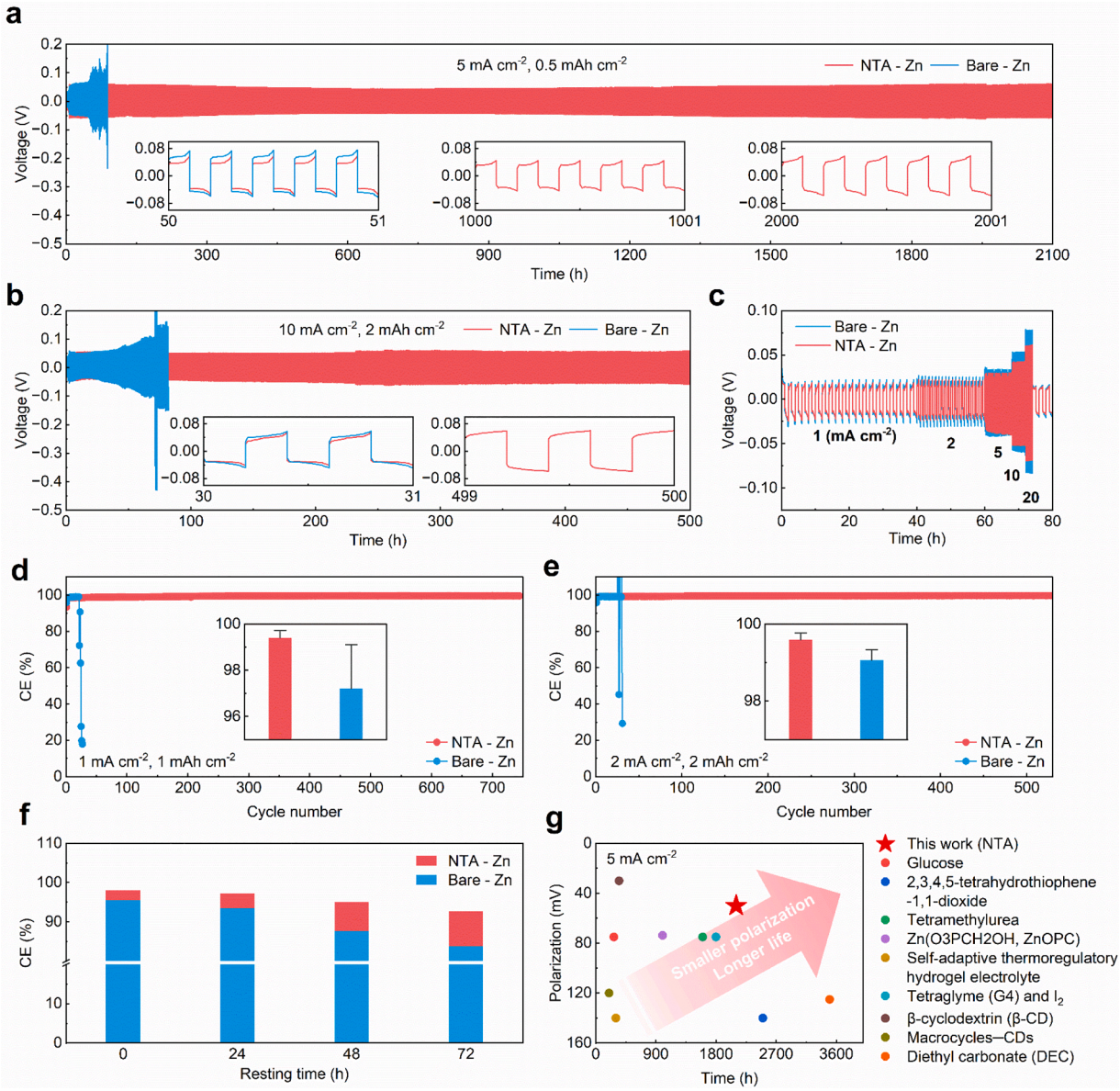

Fig. 4. Zn||Zn symmetric cell and Zn||Cu half-cell performance. (a) Cycling performance of Zn||Zn symmetric cells with 2M $ZnSO_4$ electrolyte or 2M $ZnSO_4$ +0.01M NTA electrolyte at 5 mA cm^{-2} and 0.5 mAh cm^{-2}, (b) at 10 mA cm^{-2} and 2 mAh cm^{-2}. (c) Rate performance at 1/2/5/10/20/1 mA cm^{-2}. (d) CE of Zn||Cu cells with 2M $ZnSO_4$ electrolyte or 2M $ZnSO_4$ +0.01M NTA electrolyte at 1 mA cm^{-2} and 1 mAh cm^{-2}. (e) CE of Zn||Cu cells with 2M $ZnSO_4$ electrolyte or 2M $ZnSO_4$ +0.01M NTA electrolyte at 2 mA cm^{-2} and 2 mAh cm^{-2}. (f) Average CE of Zn||Cu cells with the two different electrolytes after one deposition and resting for 0/24/48/72 h. (g) Comparison plot of cycle reversibility between this work and previous reports.

deposition, where Zn^{2+} are gradually accumulated from one to four. The stable atomic configurations and corresponding adsorption energy during this process were calculated. In all cases, the first three deposited Zn^{2+} tend to cover the Zn surface, and the aggregated state has a lower adsorption energy. When the fourth Zn^{2+} was deposited/accumulated, a stable dendrite-like structure can be formed on the NTA-free Zn surface, accompanied by a further negative value in adsorption energy (Fig. 5b). Interestingly, for both L-Zn-NTA and S-Zn-NTA surfaces, when the fourth Zn atom was added, the initial Zn dendrite-like structure was unstable, but rather spontaneously transformed into a monolayer-tiled configuration, due to a more negative value in the adsorption energy (Figs. 5c, 5d and S12). Our calculations confirm the significant inhibition of potential Zn dendrites formation via NTA and reveal the atomistic origin of uniform Zn deposition on the NTA-coated surface.

Following the outstanding performance of Zn||Zn symmetric cells and Zn||Cu cells with NTA, we tested full cell performance with MnO_2 cathode materials. As shown in Fig. 6a, the discharge capacities of these two cells were similar in the initial stage of 1C rate for the first five cycles. However, the NTA-Zn||MnO_2 cell demonstrate higher discharge capacities at various subsequent current densities. When the rate returns to 1C, the NTA-Zn||MnO_2 cell maintained a high specific capacity. In addition, the capacity retention values also showed the great advantage of NTA-Zn||MnO_2 cells, with a higher retention than Bare-Zn||MnO_2 cells at high rates (Fig. 6b). The long-term cycling performance of the two types of cells (NTA-Zn||MnO_2 cell and Bare-Zn||MnO_2 cell) at 5 mA cm^{-2} was further investigated. NTA-Zn||MnO_2 cell maintains a higher specific capacity than Bare-Zn||MnO_2 cell after 500 cycles (Fig. 6c). The discharge capacity increases in the first few cycles, which is due to the activation of the cathode material until the maximum discharge specific capacity. And as the cycle proceeds, the irreversible de-embedding of ions on the electrode and the adverse reaction of the electrolyte, etc. lead to a decrease in capacity. A higher rate the long-term cycling

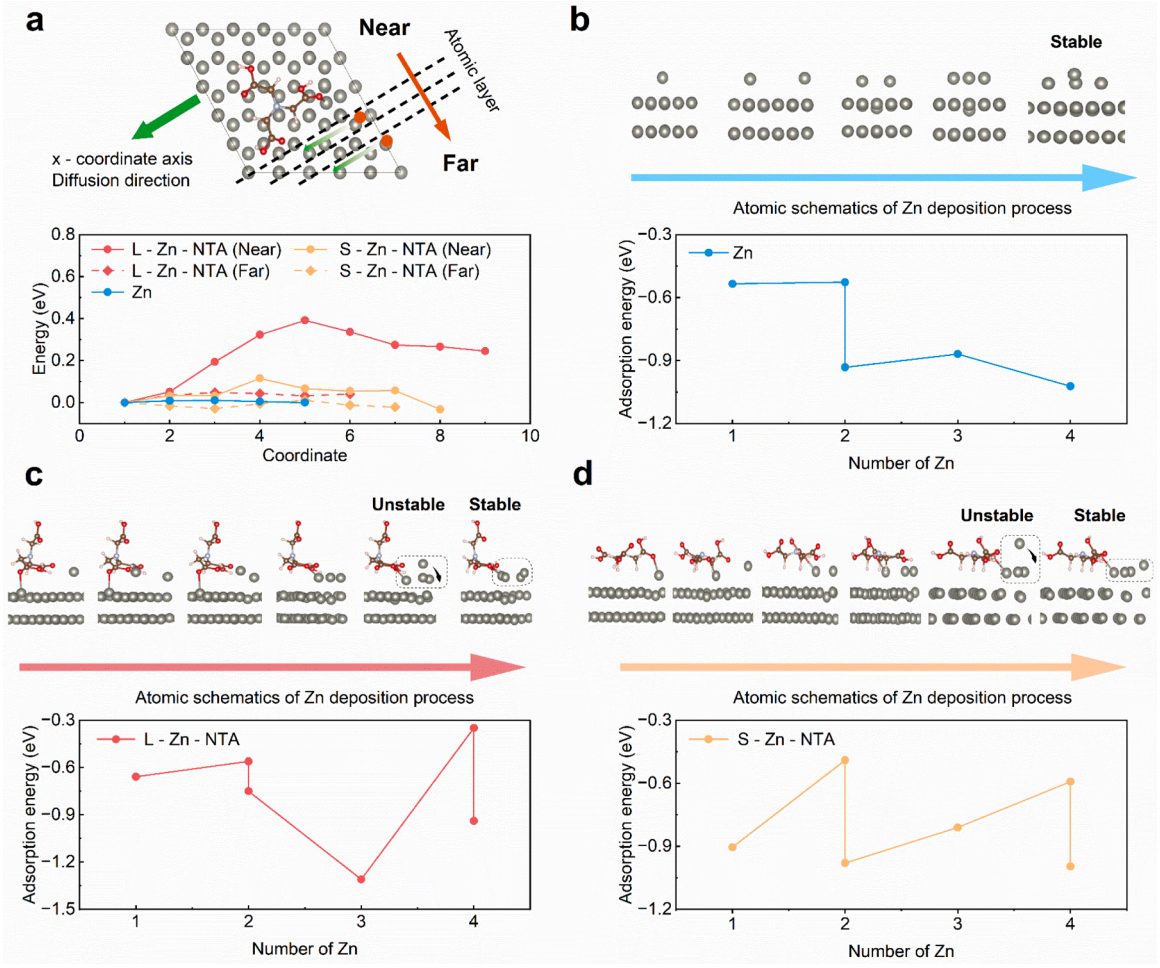

Fig. 5. DFT calculation of Zn diffusion and deposition process at Zn metal surface (a) Diffusion barriers of a single deposited Zn on L-NTA-Zn, S-NTA-Zn and Zn surfaces, where the x-axis indicates the diffusion of Zn along green arrow direction. Near and far represent the distance of deposited Zn to adsorbed NTA molecule (b–d) Atomic configurations and corresponding adsorption energy of Zn ions when the Zn ions are gradually accumulated from one to four in the three cases of L-NTA-Zn, S-NTA-Zn and Zn surfaces. The dotted box highlights the spontaneous transition of four Zn ions from a dendrite-like structure to a monolayer-tiled configuration.

performance of the two types of batteries at 10 mA cm^{-2} was also investigated (Fig. 6d). After 300 cycles, NTA-Zn||MnO_2 cell still maintains a higher specific capacity than Bare-Zn||MnO_2 cell. This can also be attributed to the multifunctional NTA on the Zn anode, which improves the anode's reversibility, stability, and ionic transportation. In addition, the performance of the two cells at different charge/discharge rates was investigated. Moreover, we assembled NTA-Zn||MnO_2 pouch cells, which we demonstrated its capability of powering a red LED light (Fig. 6e), and verified the practicability of this type of battery.

3. Conclusion

To sum up, we investigated NTA as a multifunctional electrolyte additive with a very limited amount (0.15 wt %) added in the aqueous electrolyte that can lead to excellent reversibility and stability for Zn metal batteries. This NTA additive obtains the following advantages: (1) NTA molecules can firmly adsorb on Zn metal surface, inhibiting the direct contact between Zn and water molecules, which can significantly reduce the undesired corrosion of Zn to water; (2) The NTA-rich Zn surface can preferentially desolvate Zn^{2+} ions by attracting water molecules when they shuttle through the NTA adsorption layer, and accelerate the transport of Zn^{2+}; (3) The NTA coated Zn surface could regulate the Zn deposition, where Zn^{2+} tend to deposit on the Zn surface to minimized free energy of the system, making Zn deposition more uniform and suppressing dendrites formation. These advantages are confirmed through both experiments and DFT calculations. Compared with the control group, the symmetric cell with NTA as an additive had a relatively lower polarization (about 49 mV) and an ultra-long lifetime of over 2100 h at 5 mA cm^{-2}. After up to 810 cycles, the Zn||Cu cell (NTA added) still had a high CE of up to 99.61 %. Compared with the control group, the assembled NTA - Zn || MnO_2 cell exhibited much better cycling stability for 900 cycles with 5 mA cm^{-2}. This work proposes a scalable, cost-efficient, and facile method to realize a high-performance Zn metal anode, which is helpful for developing long-cycle, practicable RAZBs.

4. Methods

4.1. Materials Preparation

The electrolyte was prepared by dissolving 3.260 g $ZnSO_4$ (99 %, McLean) and 0.019 g NTA (AR, 98.5 %, Shanghai Aladdin) into 10 mL deionized water. The control group was the same as the experimental group, except that no NTA was added. The mixture was ultrasonically stirred at 40°C for 2 h to obtain a clear and transparent solution. The experimental group was an aqueous solution of 2M $ZnSO_4$ + 0.01M NTA (that is, the mass fraction of NTA was 0.15 %), and the control group was an aqueous solution of 2M $ZnSO_4$. NTA - Zn represented the

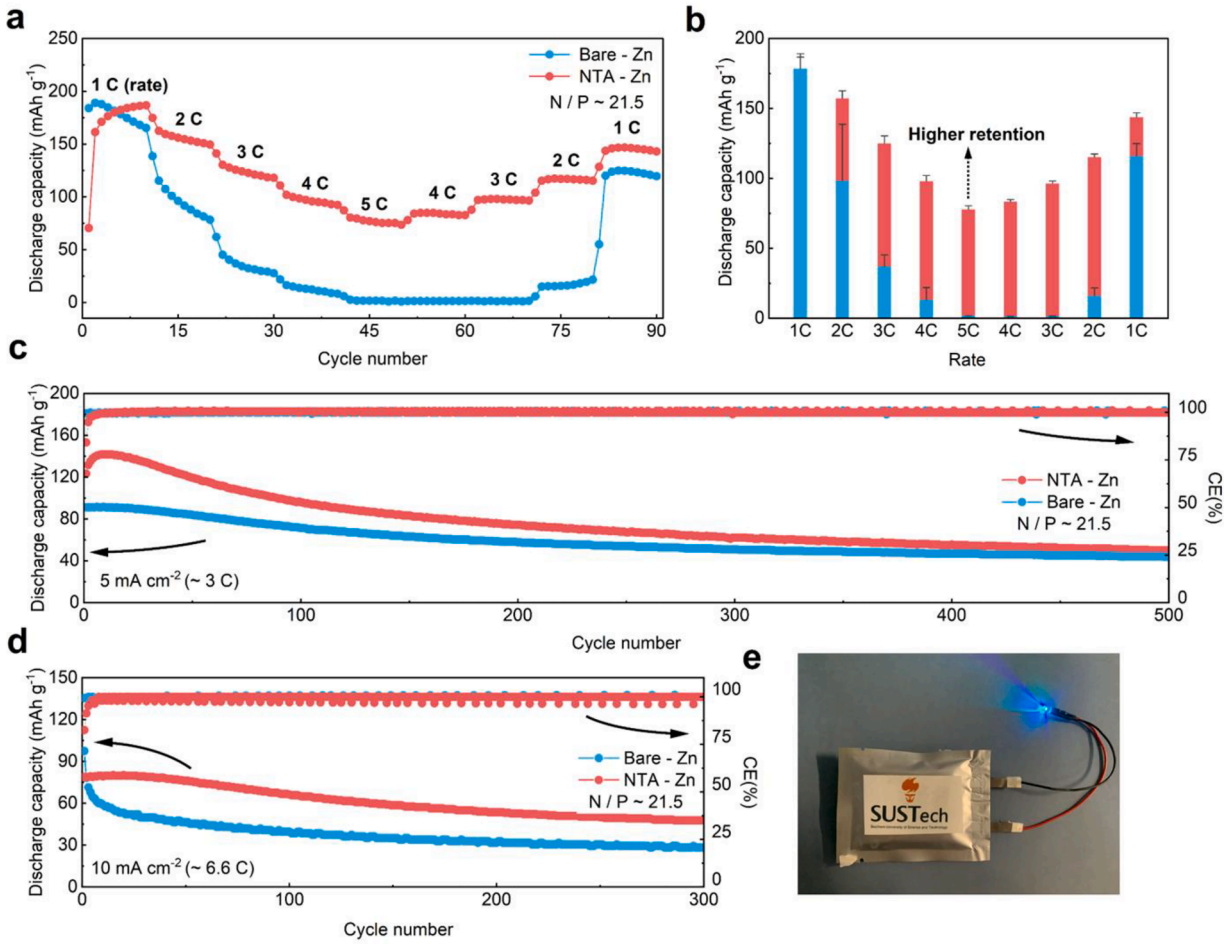

Fig. 6. Full cell performance. (a). Rate performance of the Zn-MnO_2 cell with two different electrolytes and (b) corresponding capacity retentions. Cycling performance of Zn-MnO_2 cell cycling at (c) 5 mA cm^{-2} and (d) 10 mA cm^{-2}. (e) Photo images of the NTA–Zn||MnO_2 pouch battery at different bending angles.

experimental group, and the control group was represented by Bare - Zn. The calculation method of the mass fraction of NTA was: c % = m_{NTA} / $m_{electrolyte}$, where m_{NTA} was the mass of NTA and $m_{electrolyte}$ was the total mass of the electrolyte solution. The thickness of the Zn metal foil was 200 μm, which needed to be polished with 600 - grit sandpaper first and then polished with 2000 - grit sandpaper to remove the passivation layer on the surface. And the shiny Zn metal foils were put into ethanol for 20 min and ultrasonically removed the impurities on the surface.

The linear polarization test is performed on an electrochemical workstation with a three-electrode setup. The working electrode is Zn foil, the counter electrode is graphite rod, and the reference electrode is Ag/AgCl electrode. Two types of electrolytes are utilized for the tests, namely 2M $ZnSO_4$ + 0.01M NTA and 2M $ZnSO_4$. The measurement was carried out by sweeping from -1.2V to -0.7V at a speed of 1 mV/s.

The average CE was measured with Zn-Cu cells. First, 5 mAh cm^{-2} of Zn was first deposited onto the Cu substrate and stripped from the Cu substrate in the first cycle at a current density of 1 mA cm^{-2} and a charge cutoff voltage of 0.6 V. Then, 5 mA h cm^{-2} of Zn was deposited on the Cu substrate as a Zn bank. In the next 40 cycles, 1 mA cm^{-2}, 1 mA h cm^{-2} (20 % of Zn bank, denoted as Qa) was applied for Zn stripping/deposition. Finally, the cell was charged to 0.6 V and stripped of zinc in the 41st cycle (denoted as Qc). The average CE was calculated by the following equation.

$$CE = \frac{Qc + 40*Qa}{5 + 40 * Qa} * 100\%$$

4.2. Materials characterizations

XRD was measured using a Rigaku Smartlab 9 KW X-ray diffractometer with Cu Kα radiation (45 kV, 200 mA) and a 2θ ranging from 5° to 45°. SEM and EDS images were performed with Zeiss Sigma 300. XPS was carried out with a PHI 5000 Versaprobe III. Raman characterization was performed on a LabRAM HR Evolution Raman Microspectrometer with 532 nm laser.

4.3. Electrochemical measurements

Zn||Zn symmetric cells were assembled with CR2032 type coin cell (Guangdong Canrd New Energy Technology Co.,Ltd.), zinc foil (12 mm diameter), GF/A type glass fiber separator (Whatman® syringe filters), and 2 M $ZnSO_4$ or 2 M $ZnSO_4$ + 0.01 M NTA electrolyte (130 μL). The assembled batteries were tested on a battery cycler (Neware Technology Limited) with a range of 1-50 mA cm^{-2} and 0.5-10 mAh cm^{-2}. Dynamic polarization and electrochemical impedance spectroscopy (EIS) were performed on an electrochemical workstation (Ivium Stat, IviLab 1.0.0.112). The Zn||Cu half-cell was also assembled using CR2032 type coin cell, zinc foil, copper foil, GF/A type glass fiber separator, and 2 M $ZnSO_4$ or 2 M $ZnSO_4$ + 0.01 M NTA electrolyte (130 μL). The MnO_2 cathode was prepared via a-MnO_2 (Barrett), super P, and polyvinylidene fluoride (PVDF, Aladdin) binder in a 7:2:1 weight ratio with N-methylpyrrolidone (NMP, Aladdin) as solvent. The cathode slurry was then coated on a stainless steel mesh with a loading of about 2 mg cm^{-2}. The MnO_2||Zn full cell was assembled as a CR2032 coin cell with GF/A type glass fiber separator and 2 M $ZnSO_4$ or 2 M $ZnSO_4$ + 0.01M NTA

electrolyte (130 μL).

4.4. Theoretical calculations

We carried out first-principles calculations based on density functional theory (DFT), using the Vienna ab initio simulation package (VASP) [43]. The spin-polarized generalized gradient approximation (GGA) with Perdew BurkeErnzerhof (PBE) was employed to describe the exchange-correlation function [44]. The cutoff energy for the plane-wave expansion of the wave function was set to 500 eV, and reciprocal space was sampled by the gamma-centered k-mesh with a resolution of 0.03 in the unit of 2*PI/Angstrom. The vacuum layer is at least 15 Å in the z direction to minimize possible interactions between the replicated cells. The convergence criteria are 1×10^{-5} eV energy differences for solving the electronic wave function, and the structures were relaxed until the forces on all atoms were smaller than -0.02 eV/Å. A post-stage Van der Waals DFT-D3 method with Becke-Johnson damping was applied [53]. Climbing image nudged elastic band (CI-NEB) method to seek the minimum energy path and saddle points in the calculation of Zn ion diffusion [54].

Supporting Information

S1. pH tests; S2. SEM images of bare-Zn; S3. 3D views of charge density difference and bader charge; S4. Partial density of states; S5–S9. XPS spectrums; S10,S11. Voltage profiles of symmetric cells; S12. Energy change from the initial Zn dendrite to the tiled structure calculated from the NEB method and the evolution of the atomic structure.

CRediT authorship contribution statement

Zhenye Liang: Conceptualization, Methodology, Validation, Formal analysis, Investigation, Data curation, Writing – original draft. **Chao Li:** Conceptualization, Formal analysis, Data curation, Investigation, Writing – original draft. **Daxian Zuo:** Visualization, Writing – review & editing. **Lin Zeng:** Conceptualization, Writing – review & editing. **Tong Ling:** Visualization. **Jiajia Han:** Software, Validation, Visualization, Supervision, Writing – original draft. **Jiayu Wan:** Conceptualization, Resources, Funding acquisition, Project administration, Supervision, Writing – review & editing.

Declaration of Competing Interest

The authors declare that they have no known competing financial interests or personal relationships that could have appeared to influence the work reported in this paper.

Acknowledgments

This work is funded by National Natural Science Foundation of China (52272215), Shenzhen Science and Technology Program (JCYJ20220818100218040).

Supplementary materials

Supplementary material associated with this article can be found, in the online version, at doi:10.1016/j.ensm.2023.102980.

References

[1] MM Thackeray, C Wolverton, ED. Isaacs, Electrical energy storage for transportation—approaching the limits of, and going beyond, lithium-ion batteries, Energy Environ. Sci. 5 (7) (2012) 7854–7863, https://doi.org/10.1039/c2ee21892e.
[2] B Diouf, R. Pode, Potential of lithium-ion batteries in renewable energy, Renew. Energy 76 (2015) 375–380, https://doi.org/10.1016/j.renene.2014.11.058.
[3] MK Hasan, M Mahmud, AA Habib, S Motakabber, S. Islam, Review of electric vehicle energy storage and management system: standards, issues, and challenges, J. Energy Storage. 41 (2021), 102940, https://doi.org/10.1016/j.est.2021.102940.
[4] E Pomerantseva, F Bonaccorso, X Feng, Y Cui, Y. Gogotsi, Energy storage: the future enabled by nanomaterials, Science 366 (6468) (2019) eaan8285, https://doi.org/10.1126/science.aan8285.
[5] Z Zhu, T Jiang, M Ali, Y Meng, Y Jin, Y. Cui, Rechargeable batteries for grid scale energy storage, Chem. Rev. 122 (22) (2022) 16610–16751, https://doi.org/10.1021/acs.chemrev.2c00289.
[6] S Xia, X Wu, Z Zhang, Y Cui, W. Liu, Practical challenges and future perspectives of all-solid-state lithium-metal batteries, Chemistry 5 (4) (2019) 753–785, https://doi.org/10.1016/j.chempr.2018.11.013.
[7] K Liu, Y Liu, D Lin, A Pei, Y. Cui, Materials for lithium-ion battery safety, Sci. Adv. 4 (6) (2018) eaas9820, https://doi.org/10.1126/sciadv.aas9820.
[8] Y Li, Z Wang, Y Cai, ME Pam, Y Yang, D. Zhang, Designing advanced aqueous zinc-ion batteries: principles, strategies, and perspectives, Energy Environ. Mater. 5 (3) (2022) 823–851, https://doi.org/10.1002/eem2.12265.
[9] Y Chen, Y Kang, Y Zhao, L Wang, J Liu, Y. Li, A review of lithium-ion battery safety concerns: the issues, strategies, and testing standards, J. Energy Chem. 59 (2021) 83–99, https://doi.org/10.1016/j.jechem.2020.10.017.
[10] Q Wang, L Jiang, Y Yu, J. Sun, Progress of enhancing the safety of lithium ion battery from the electrolyte aspect, Nano Energy 55 (2019) 93–114, https://doi.org/10.1016/j.nanoen.2018.10.035.
[11] L Kang, M Cui, Z Zhang, F. Jiang, Rechargeable aqueous zinc-ion batteries with mild electrolytes: a comprehensive review, Batter. Super. 3 (10) (2020) 966–1005, https://doi.org/10.1002/batt.202000060.
[12] M Wu, G Zhang, H Yang, X Liu, M Dubois, MA. Gauthier, Aqueous Zn-based rechargeable batteries: recent progress and future perspectives, InfoMat 4 (5) (2022) e12265, https://doi.org/10.1002/inf2.12265.
[13] Z Cai, J Wang, Y. Sun, Anode corrosion in aqueous Zn metal batteries, eScience 3 (2023), 100093, https://doi.org/10.1016/j.esci.2023.100093.
[14] Y Liu, Y Liu, X. Wu, Toward long-life aqueous zinc ion batteries by constructing stable zinc anodes, Chem. Rec. 22 (10) (2022), e202200088, https://doi.org/10.1002/tcr.202200088.
[15] F Wang, H Lu, H Li, J Li, L Wang, D. Han, Demonstrating U-shaped zinc deposition with 2D metal-organic framework nanoarrays for dendrite-free zinc batteries, Energy Stor. Mater. 50 (2022) 641–647, https://doi.org/10.1016/j.ensm.2022.06.005.
[16] L Wang, Z Wang, H Li, D Han, X Li, F. Wang, Aminosilane molecular layer enables successive capture-diffusion-deposition of ions toward reversible zinc electrochemistry, ACS nano 17 (1) (2022) 668–677, https://doi.org/10.1021/acsnano.2c09977.
[17] P Sun, L Ma, W Zhou, M Qiu, Z Wang, D. Chao, Simultaneous regulation on solvation shell and electrode interface for dendrite-free Zn ion batteries achieved by a low-cost glucose additive, Angew. Chem. Int. Ed. 133 (33) (2021) 18395–18403, https://doi.org/10.1002/anie.202105756.
[18] M Wang, Y Meng, K Li, T Ahmad, N Chen, Y. Xu, Toward dendrite-free and anti-corrosion Zn anodes by regulating a bismuth-based energizer, eScience 2 (5) (2022) 509–517, https://doi.org/10.1016/j.esci.2022.04.003.
[19] J Zheng, LA. Archer, Controlling electrochemical growth of metallic zinc electrodes: Toward affordable rechargeable energy storage systems, Sci. Adv. 7 (2) (2021) eabe0219, https://doi.org/10.1126/sciadv.abe0219.
[20] Y Du, Y Li, BB Xu, TX Liu, X Liu, F. Ma, Electrolyte salts and additives regulation enables high performance aqueous zinc ion batteries: a mini review, Small 18 (43) (2021), 2104640, https://doi.org/10.1002/smll.202104640.
[21] TK Hoang, M Acton, HT Chen, Y Huang, TNL Doan, P. Chen, Sustainable gel electrolyte containing Pb^{2+} as corrosion inhibitor and dendrite suppressor for the zinc anode in the rechargeable hybrid aqueous battery, Mater. Today Energy. 4 (2017) 34–40, https://doi.org/10.1016/j.mtener.2017.03.003.
[22] D Zhang, J Cao, X Zhang, N Insin, S Wang, J. Han, Inhibition of manganese dissolution in Mn_2O_3 cathode with controllable Ni^{2+} incorporation for high-performance zinc ion battery, Adv. Funct. Mater. 31 (14) (2021), 2009412, https://doi.org/10.1002/adfm.202009412.
[23] G Zhang, X Zhang, H Liu, J Li, Y Chen, H. Duan, 3D-printed multi-channel metal lattices enabling localized electric-field redistribution for dendrite-free aqueous Zn ion batteries, Adv. Energy Mater. 11 (19) (2021), 2003927, https://doi.org/10.1002/aenm.202003927.
[24] X Xu, Y Chen, D Zheng, P Ruan, Y Cai, X. Dai, Ultra-fast and scalable saline immersion strategy enabling uniform Zn nucleation and deposition for high-performance Zn-ion batteries, Small 17 (33) (2021), 2101901, https://doi.org/10.1002/smll.202101901.
[25] K Owusu, X Pan, R Yu, L Qu, Z Liu, Z. Wang, Introducing Na_2SO_4 in aqueous $ZnSO_4$ electrolyte realizes superior electrochemical performance in zinc-ion hybrid capacitor, Mater. Today Energy 18 (2020), 100529, https://doi.org/10.1016/j.mtener.2020.100529.
[26] Y Xu, J Zhu, J Feng, Y Wang, X Wu, P. Ma, A rechargeable aqueous zinc/sodium manganese oxides battery with robust performance enabled by Na_2SO_4 electrolyte additive, Energy Stor. Mater. 38 (2021) 299–308, https://doi.org/10.1016/j.ensm.2021.03.019.
[27] Y Li, Y Yang, X Liu, Y Yang, Y Wu, L. Han, Flexible self-powered integrated sensing system based on a rechargeable zinc-ion battery by using a multifunctional polyacrylamide/carboxymethyl chitosan/LiCl ionic hydrogel, Colloids Surf 648 (2022), 129254, https://doi.org/10.1016/j.colsurfa.2022.129254.
[28] X Guo, Z Zhang, J Li, N Luo, G.L Chai, TS. Miller, Alleviation of dendrite formation on zinc anodes via electrolyte additives, ACS Energy Lett 6 (2) (2021) 395–403, https://doi.org/10.1021/acsenergylett.0c02371.

[29] Y Geng, L Pan, Z Peng, Z Sun, H Lin, C. Mao, Electrolyte additive engineering for aqueous Zn ion batteries, Energy Stor. Mater. 55 (2022) 733–755, https://doi.org/10.1016/j.ensm.2022.07.017.
[30] C Qiu, X Zhu, L Xue, M Ni, Y Zhao, B. Liu, The function of Mn^{2+} additive in aqueous electrolyte for Zn/δ-MnO_2 battery, Electrochim. Acta. 351 (2020), 136445, https://doi.org/10.1016/j.electacta.2020.136445.
[31] V Soundharrajan, B Sambandam, S Kim, S Islam, J Jo, S Kim, The dominant role of Mn^{2+} additive on the electrochemical reaction in $ZnMn_2O_4$ cathode for aqueous zinc-ion batteries, Energy Stor. Mater. 28 (2020) 407–417, https://doi.org/10.1016/j.ensm.2019.12.021.
[32] Z Liu, L Qin, B Lu, X Wu, S Liang, J. Zhou, Issues and opportunities facing aqueous Mn^{2+}/MnO^{2-}based batteries, ChemSusChem 15 (10) (2022), e202200348, https://doi.org/10.1002/cssc.202200348.
[33] Y Ou, Z Cai, J Wang, R Zhan, S Liu, Z. Lu, Reversible aqueous Zn battery anode enabled by a stable complexation adsorbent interface, EcoMat 4 (3) (2022) e12167, https://doi.org/10.1002/eom2.12167.
[34] V Filipe, A Hawe, W. Jiskoot, Critical evaluation of nanoparticle tracking analysis (NTA) by NanoSight for the measurement of nanoparticles and protein aggregates, Pharm. Res. 27 (5) (2010) 796–810, https://doi.org/10.1007/s11095-010-0073-2.
[35] A Kayser, K Wenger, A Keller, W Attinger, H Felix, S. Gupta, Enhancement of phytoextraction of Zn, Cd, and Cu from calcareous soil: the use of NTA and sulfur amendments, Environ. Sci. Technol. 34 (9) (2000) 1778–1783, https://doi.org/10.1021/es990697s.
[36] AC Alder, H Siegrist, W Gujer, W. Giger, Behaviour of NTA and EDTA in biological wastewater treatment, Water Res 24 (6) (1990) 733–742, https://doi.org/10.1016/0043-1354(90)90029-6.
[37] J Hao, X Li, X Zeng, D Li, J Mao, Z. Guo, Deeply understanding the Zn anode behaviour and corresponding improvement strategies in different aqueous Zn-based batteries, Energy Environ. Sci. 13 (11) (2020) 3917–3949, https://doi.org/10.1039/d0ee02162h.
[38] L Hu, P Xiao, L Xue, H Li, T. Zhai, The rising zinc anodes for high-energy aqueous batteries, EnergyChem 3 (2) (2021), 100052, https://doi.org/10.1016/j.enchem.2021.100052.
[39] A Mitha, AZ Yazdi, M Ahmed, P. Chen, Surface adsorption of polyethylene glycol to suppress dendrite formation on zinc anodes in rechargeable aqueous batteries, ChemElectroChem 5 (17) (2018) 2409–2418, https://doi.org/10.1002/celc.201800572.
[40] R Meng, H Li, Z Lu, C Zhang, Z Wang, Y. Liu, Tuning Zn-Ion solvation chemistry with chelating ligands toward stable aqueous Zn Anodes, Adv. Mater. 34 (37) (2022), 2200677, https://doi.org/10.1002/adma.202200677.
[41] J Yang, Y Zhang, Z Li, X Xu, X Su, J. Lai, Three birds with one stone: tetramethylurea as electrolyte additive for highly reversible Zn-metal anode, Adv. Funct. Mater. 32 (2022), 2209642, https://doi.org/10.1002/adfm.202209642.
[42] K Xie, K Ren, C Sun, S Yang, M Tong, S. Yang, Toward stable zinc-ion batteries: use of a chelate electrolyte additive for uniform zinc deposition, ACS Appl. Energy Mater. 5 (4) (2022) 4170–4178, https://doi.org/10.1021/acsaem.1c03558.
[43] J Zhou, F Wu, Y Mei, Y Hao, L Li, M. Xie, Establishing thermal infusion method for stable zinc metal anodes in aqueous zinc-ion batteries, Adv. Mater. 34 (21) (2022), 2200782, https://doi.org/10.1002/adma.202200782.
[44] BD Adams, J Zheng, X Ren, W Xu, JG. Zhang, Accurate determination of coulombic efficiency for lithium metal anodes and lithium metal batteries, Adv. Energy Mater. 8 (7) (2018), 1702097, https://doi.org/10.1002/aenm.201702097.
[45] K Zhao, G Fan, J Liu, F Liu, J Li, X. Zhou, Boosting the kinetics and stability of Zn anodes in aqueous electrolytes with supramolecular cyclodextrin additives, J. Am. Chem. Soc. 144 (25) (2022) 11129–11137, https://doi.org/10.1021/jacs.2c00551.
[46] He J, Tang Y, Liu G, Li H, Ye M, Zhang Y. Intrinsic hydrogen-bond donors-lined organophosphate superionic nanochannels levering high-rate-endurable aqueous Zn batteries. Adv. Energy Mater. 12:2202661. 10.1002/aenm.202202661.
[47] M Zhou, S Guo, J Li, X Luo, Z Liu, T. Zhang, Surface-preferred crystal plane for a stable and reversible zinc anode, Adv. Mater. 33 (21) (2021), 2100187, https://doi.org/10.1002/adma.202100187.
[48] M Qiu, P Sun, Y Wang, L Ma, C Zhi, W. Mai, Anion-trap engineering toward remarkable crystallographic reorientation and efficient cation migration of Zn ion batteries, Angew. Chem. Int. Ed. 61 (44) (2022), e202210979, https://doi.org/10.1002/anie.202210979.
[49] K Wang, T Qiu, L Lin, X.X Liu, X. Sun, A low fraction electrolyte additive as interface stabilizer for Zn electrode in aqueous batteries, Energy Stor. Mater. 54 (2022) 366–373, https://doi.org/10.1016/j.ensm.2022.10.029.
[50] Y Meng, L Zhang, M Peng, D Shen, C Zhu, S. Qian, Developing thermoregulatory hydrogel electrolyte to overcome thermal runaway in zinc-ion batteries, Adv. Funct. Mater. 32 (46) (2022), 2206653, https://doi.org/10.1002/adfm.202206653.
[51] Z Zhu, M Yang, Z Yan, J Xiao, W Xin, L. Zhang, Boosting cathode activity and anode stability of Zn-S batteries in aqueous media through cosolvent-catalyst synergy, Angew. Chem. Int. Ed. 134 (2022), e202212, https://doi.org/10.1002/anie.202212666.
[52] L Miao, R Wang, S Di, Z Qian, L Zhang, W. Xin, Aqueous electrolytes with hydrophobic organic cosolvents for stabilizing zinc metal anodes, ACS Nano 16 (6) (2022) 9667–9678, https://doi.org/10.1021/acsnano.2c02996.
[53] S Grimme, S Ehrlich, L. Goerigk, Effect of the damping function in dispersion corrected density functional theory, J. Comput. Chem. 32 (7) (2011) 1456–1465, https://doi.org/10.1002/jcc.21759.
[54] G Henkelman, BP Uberuaga, H. Jónsson, A climbing image nudged elastic band method for finding saddle points and minimum energy paths, J. Chem. Phys. 113 (22) (2000) 9901–9904, https://doi.org/10.1063/1.1329672.